

Journal of Materials Chemistry A

Accepted Manuscript



This is an *Accepted Manuscript*, which has been through the Royal Society of Chemistry peer review process and has been accepted for publication.

Accepted Manuscripts are published online shortly after acceptance, before technical editing, formatting and proof reading. Using this free service, authors can make their results available to the community, in citable form, before we publish the edited article. We will replace this *Accepted Manuscript* with the edited and formatted *Advance Article* as soon as it is available.

You can find more information about *Accepted Manuscripts* in the [Information for Authors](#).

Please note that technical editing may introduce minor changes to the text and/or graphics, which may alter content. The journal's standard [Terms & Conditions](#) and the [Ethical guidelines](#) still apply. In no event shall the Royal Society of Chemistry be held responsible for any errors or omissions in this *Accepted Manuscript* or any consequences arising from the use of any information it contains.

Cite this: DOI: 10.1039/c0xx00000x

www.rsc.org/xxxxxx

ARTICLE TYPE

Novel porous MgO sorbent fabricated through carbon-insertion

Yan Yan Li^a, Mi Mi Wan^a, Wei Gang Lin^a, Ying Wang^{b, c}, Jian Hua Zhu^{*a}

Received (in XXX, XXX) Xth XXXXXXXXXX 20XX, Accepted Xth XXXXXXXXXX 20XX

DOI: 10.1039/b000000x

5 Abstract: A new strategy of “carbon insertion” to synthesize a high efficient CO₂-capturer through self-dispersion of MgO by co-existed carbon is reported in this article. Carbon-adulterated magnesia is in situ formed in the carbonization of magnesium acetate for the first time, suppressing the aggregation of MgO nano-particles and increasing the accessibility of basic sites for CO₂. With few carbon particles (about 2%) inside as the adulterant, the porous MgO composites have a surface area of above 200 m² g⁻¹ and a high adsorption capacity of CO₂ up to 28 mg g⁻¹ at 473 K, offering a new candidate for adsorbing CO₂ in flue gas vent.

10 Introduction

Controlling greenhouse gas CO₂ emission is a key target in the fight against global climate warming. The concentration of atmospheric CO₂ has a remarkable growth from about 310 to over 380 ppm in the last half century,¹ and combustion of fossil energy resource is the main cause because 94% of CO₂ comes from carbon-based fossil fuels in United States.² Therefore, how to capture and sequester CO₂ from major anthropogenic sources such as coal-fired power plants becomes a hot-point of research.³

Various materials and technologies are tried for reducing the CO₂ emission but their applications are hindered by the temperature of flue gas vent, which is usually in the range of 423–673 K.⁵ Amine-modified materials suffer from the drawback of volatilization and thermal degradation,⁶ zeolites, hydroxalite and metal organic frameworks are weak to capture CO₂ at the elevated temperature, while Li-based or Ca-based sorbents are limited by their high regeneration temperature (1073–1173 K).⁷ It is necessary to fabricate a proper basic sorbent capturing CO₂ above 423 K and being regenerated below 773 K, and MgO is recognized as the promising candidate because of its suitable basic strength along with high CO₂ adsorption capacity and low energy requirement for regeneration.⁸

MgO has been widely used in catalysis, refractory material industries, sorbent and superconductors, but its potential application as CO₂ sorbent is obstructed by its low surface area-to-volume ratio and the formation of a termination layer of carbonate on the surface, which is a hindrance toward further reaction of MgO with CO₂.^{9–11} It is vital to decrease the particle size of MgO and increase the exposure of active sites, for which three strategies are adopted to enhance the adsorptive efficiency of MgO. The first one intends to disperse MgO on porous support, forming various new sorbents such as porous carbon supported MgO,^{12, 13} MgO/Al₂O₃ sorbent,^{14, 15} mesoporous MgO/carbon composites,¹⁶ and MgO/TiO₂ mixed oxides.⁸ Nonetheless, the efficiency of these MgO supported materials in CO₂ adsorption is restricted by the proportion of support. Most of the supports are inactive for CO₂ adsorption therefore their existence will inevitably reduce the adsorption capacity of per gram sorbent.

Besides, the well-dispersed MgO on zeolite or mesoporous silica cannot keep its original crystals and often fails to show a strong basicity,^{17–19} since the defects on MgO crystal provide the strong basic active sites to adsorb CO₂.^{13, 20} The second strategy is to directly synthesize porous MgO through replica or pore-creating methods, enhancing the surface area-to-volume ratio and expose more active sites,^{11, 21, 22} but they need the assistance of surfactant agents and the costly multi-step fabrication procedures. A lot of effort has been performed in the third strategy to prepare the MgO nano-particles using special raw materials like magnesium methyrate,^{23–25} yet these extra-fine particles are aggregated at high temperature, resulting in a declined performance in CO₂ adsorption. Hence new synthetic strategy of efficient MgO adsorbent is sought, in order to get the new porous sorbent with four characters: (1) The MgO nanoparticles keep their original crystals. (2) They are separated by adulterant so that they can be farthest exposed. (3) The adulterant should have a light molecular weight and its proportion in the sorbent should be minimized. (4) The formation and separation of MgO particles should be performed simultaneously.

Recently we observed the formation of self-dispersed MgO on the activated carbon impregnated with magnesium acetate.¹³ The magnesia and carbon mixed particles were in situ formed in the carbonization of magnesium acetate on the activated carbon, which slightly increased the accessibility of basic sites for CO₂ at 373 and 423 K. Similarly, the carbon formed from the carbonization of surfactant has been used as the archer to form the pore in MgO sorbent, although the carbon was removed finally.²¹ These phenomena provide a clue for the fabrication of new porous MgO sorbent with the assistance of the co-exist carbon fine particles, here named as “carbon insertion”, offering a new solvent-free route through the carbonization of magnesium acetate: the inherent carbon source of magnesium acetate will be utilized to produce lots of carbon nanoparticles during the carbonation procedure, and the carbon will be in situ embedded in the newly formed MgO nanoparticles to separate them and thus create pores or gaps in the resulting composite, fabricating a novel porous MgO composite through the special “isolation” manner to minimize the proportion of the carbon adulterant and

elevate the adsorptive efficiency of sorbent. To critically assess the actual performance of resulting MgO-based sample, the instantaneous adsorption method accompanied with the static adsorption of CO₂ at 473 K is employed.¹³ Capture of CO₂ at 473 K is a real challenge for MgO sorbent since this temperature is lower than that required for formation of carbonate.²⁶ In order to explore how the anion of precursor salt affects the fabrication and adsorption performance of porous MgO sorbent, magnesium nitrate is also used as different raw material for comparison.

10 Experimental

Materials

Magnesium acetate tetrahydrate and magnesium nitrate hexahydrate were the product of Sinopharm Chemical Reagent (China). All chemicals are used as received without further purification.

Synthesis of porous MgOs

Certain amount of Mg(CH₃COO)₂•4H₂O was mounted in the u-type quartz tube with a length of 18 cm and internal diameter of 3 mm, then heated in a flow of N₂ (99.995%, 30 ml min⁻¹) at 623, 673, 723, 773, 823 and 873 K for 2h, the obtained samples were denoted as MA-n (n=1~6), respectively. Similarly, the sample derived from thermal decomposed Mg(NO₃)₂•6H₂O in the u-type quartz tube in N₂ at 823 K was named as MN. Besides, magnesium acetate was carbonized in a tube furnace with an internal diameter of 5 cm at 823 K in the N₂ flow of 0.3 L min⁻¹ for 4h, giving the sample named as MA-5t. In case the N₂ flow was changed to air, samples MA-5t-a and MA-5-a were prepared. When the sample was carbonized in u-type at 823 K in N₂ atmosphere instead of N₂ flow, the resulting same was named as MA-5-s.

Characterizations

X-ray diffraction (XRD) patterns of samples were recorded on an ARL XTRA diffractometer (power 40 kV, 40 mA) using Cu-K α radiation in the 2-theta range from 0.5° to 8° or from 6° to 90°. Crystallite size of samples were calculated through Scherrer equation: $L=0.89\lambda/B(2\theta)\cos\theta$, where B(2 θ) is the width at half peak-height in the X-ray pattern line in radian, λ is the wavelength of the Cu K α (0.154056 nm), θ is the diffraction angle in degrees, and L is the crystallite size of the samples in nanometers.

Nitrogen adsorption-desorption isotherms were measured on a Micromeritics ASAP 2020 system at 77 K, and the sample was evacuated at 573 K for 4 h prior to test. The Brunauer–Emmett–Teller (BET) method was utilized to calculate the specific surface area of sample using adsorption branch acquired at a relative pressure (P/P₀) range of 0.05-0.22, and the total pore volume was estimated from the amount adsorbed at a relative pressure (P/P₀) of 0.98. Elemental Analysis was conducted on Heraeus-CHN-O-Rapid instrument, and TEM analysis was carried out on a JEM-1011 electron microscope operating at 200 kV.¹⁸ SEM images, elemental mapping and EDX analysis of samples were obtained on Hitachi S4800 microscopes at 20 kV, 10 μ A. X-Ray photoelectron spectra (XPS) were recorded on a VG Escalab MK II system equipped with a hemispherical electron analyzer, using non-monochromatic Mg

K α radiation (1253.6 eV).

To monitor the thermal decomposition of magnesium acetate, 214 mg of the salt was heated in the u-type quartz tube from room temperature to 823 K at a rate of 2 K min⁻¹ with a flow of N₂ (5 ml min⁻¹), and kept at 823 K for 4 h, meanwhile the gaseous products were detected by an Ametek Dycor LC-D200 MS instrument.

The in situ Fourier transform infrared (FT-IR) spectra of CO₂ adsorbed on the porous MgO samples were recorded on a Nicolet 5700 FT-IR spectrometer equipped with a DTGS detector with a resolution of 4 cm⁻¹.⁴¹ The sample was pressed into a self-supporting wafer (about 15 mg cm⁻²), and mounted in a commercial controlled environment chamber (HTC-3). The sample disc was thermally activated to 773 K at the rate of 8 K min⁻¹ in N₂ flow for 2 h. After the sample was cooled to 473 K to take a background spectrum, it was exposed to a stream of CO₂ at a rate of 10 ml min⁻¹ for 20 min, followed by a purge of N₂ for 10 min to remove the physical adsorbed CO₂ prior to recording the FTIR spectrum. Then the sample was heated from 473 to 673 K at a rate of 10 K min⁻¹, and the FT-IR spectrum was recorded at a given temperatures.

To assess the performance of sample in instantaneous CO₂ adsorption at 473 K,¹³ the in situ prepared sample (about 20 mg) in u-type quartz tube was kept to 473 K, and 0.164 mL of CO₂ was injected each time accompanied with carrier gas (30 ml min⁻¹). The residual CO₂ was detected by an “online” Varian 3380 gas chromatograph and quantitatively measured by the external standard method¹⁵. Once the adsorption was finished, the sample was purged with a N₂ flow for 10 min, and then heated from 473 to 673 K and hold at 673 K for 1 h, meanwhile the liberated products were detected by an Ametek Dycor LC-D200 MS together with the “online” Varian 3380 gas chromatograph. In the cyclic adsorption-desorption experiments, the sample was allowed to re-adsorb CO₂ in the same manner aforementioned as soon as the entire desorption process was finished.

The CO₂ adsorption isotherm was measured using a Micromeritics ASAP 2020 static volumetric analyzer at the setting temperature^{13, 21}. Prior to adsorption experiment, the sample was degassed at 673 K for 6 h, and then cooled down to the target temperature, followed by introduction of CO₂ into the system. The gas adsorption amount was then recorded in terms of adsorbed volume under standard temperature and pressure (STP).

Results

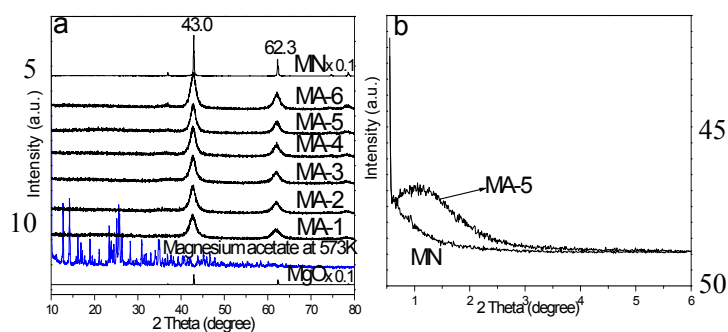
100 Fabrication of mesoporous MgO from carbonization of magnesium acetate

Table 1 reports the carbonization temperature and textural property of porous MgO samples. All of the MA-n samples prepared in 623-873 K had the XRD diagram of crystalline MgO characterized with two peaks at 2-theta value of 43.0° and 62.3° (Fig. 1a),^{11, 13, 15} indicating the decomposition of magnesium acetate. These two peaks became slightly stronger meanwhile the width of the former was marginally reduced as the carbonized temperature increased from 623 to 873 K, probably concerning in the arrangement of MgO nanoparticles at high temperature.²⁵ Also, magnesium nitrate was fully decomposed at 823 K so that the characteristics of MgO with the very thin and strong peaks were observed in the XRD pattern of MN sample (Fig. 1a).

Table 1. Textural properties of the prepared MgO samples and their CO₂ adsorption capacities at 473 K.

Samples	Temp. treated (K)	Pore volume (cm ³ g ⁻¹)	Pore size ^[a] (nm)	BET surface area (m ² g ⁻¹)	Crystallite size L _{62(2θ)} (nm)	Carbon Content (%)	CO ₂ adsorbed at 473 K (mg g ⁻¹)
MA-1	623	0.22	1.8	235.8	4.7±2	8.3±0.1	<1
MA-2	673	0.22	3.1	271.5	5.5±2	2.9±0.1	20.8
MA-3	723	0.20	1.9	317.3	5.4±2	2.3±0.3	26.6
MA-4	773	0.27	3.0	317.8	5.7±2	2.1±0.1	27.5
MA-5	823	0.25	3.5	300.8	7.0±2	2.5±0.4	27.7
MA-6	873	0.34	3.3	336.1	5.6±2	1.8±0.7	28.9
MN	823	0.01	3.3	11.2	54.0±2	0	4.2
MA-5t	823	0.20	3.3	225.3	17.7±2	0.75±0.1	15.1
MA-5t-a	823	0.13	10.7	42.6	18.4±2	0	7.5
MA-5-a	823	0.21	3.2	148.8	9.2±2	0	19.8
MA-1-a	623	0.15	3.7	135.5	7.6±2	5.1±0.1	3.3
MA-5-s	823	0.20	23.2	35.3	23.5±2	4.3±0.1	8.1

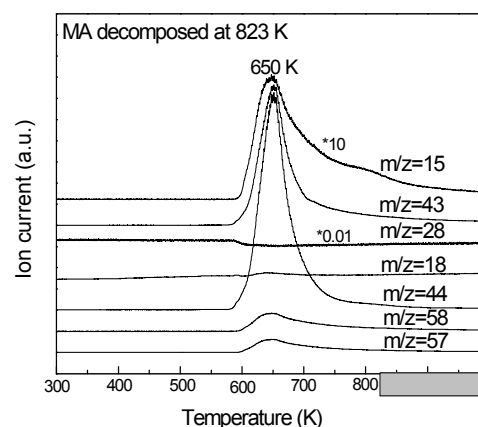
[a] This is obtained by the peak position of the pore size distribution.



15 **Fig. 1** Wide-angle (a) and low-angle (b) XRD patterns of MA-n and MN samples.

Usually magnesium acetate becomes glassy state at 353 K in calcination,²⁷ and then it is dehydrated followed by the decomposition in 596–623 K,^{11, 28} producing CO₂, acetone and MgO. According to mass ion detection, however, gaseous products were released around 650 K in the carbonization of magnesium acetate (Fig. 2), including CO₂ (m/z = 44), H₂O (m/z = 18) and acetone (m/z = 58, 57, 43, 15), meanwhile lots of MgO nanoparticles were produced to form the wide peaks of diffraction in the XRD pattern as demonstrated in Fig. 1a. The crystallites sizes of MA-n samples, calculated from the line broadening of the peak at 62° (2-theta) using the Scherrer equation $L_{62(2\theta)}$, were in the range of 5–7 nm (Table 1), similar to that prepared from magnesium methyle (4–7 nm).²⁵ On the other hand, one diffraction peak with 2-theta value of about 1.1° was observed on the low-angle XRD pattern of MA-5 sample (Fig. 1b), mirroring a declined mesoporous structure with no long-range order; and similar cumulate pore structure had been found on the composite with microcrystalline MgO dispersed in the framework of alumina to form a concrete-like structure.¹⁵ Dissimilarly, no mesoporous pore was found on MN sample.

Two types of nitrogen adsorption isotherms were observed on MA-n samples (Fig. 3a). A kind of type II isotherm was found on the samples of MA-1, MA-2 and MA-3, while MA-4, MA-5 and MA-6 composites had a type IV one in which the hysteresis loop



55 **Fig. 2** Mass Spectrum signals of the decomposed products while magnesium acetate was heated from room temperature to 823 K.

became clear to a higher degree. Among them MA-5 and MA-6 samples presented unapparent hysteresis loop between relative pressures of 0.4 to 0.8, testifying the relatively lowered mesoporous structure.¹¹ TEM image confirmed the successful pore-creating in MA-5 sample where worm-like pores with irregular shape were observed (Fig. 4a), and these randomly arranged pores implied the disordered mesoporous structure.¹¹ Such pore-creating is controllable and repeatable because the MA-5 composite could be repeatable prepared as demonstrated in Fig. 3b.

Carbonization temperature of magnesium acetate strongly impacts the pore formation of MA-n sample. As the temperature was lifted from 623 to 873 K, the surface area of MA-n sample increased from 235 to 336 m² g⁻¹ (Table 1), much larger than that of foam-like MgO (101–121 m² g⁻¹)²¹ and mesoporous MgO (120–136 m² g⁻¹)¹¹ as well as common MgO (about 10 m² g⁻¹)^{15, 21}, and close to that of ordered mesoporous MgO through replica method (250–306 m² g⁻¹).^{22, 29} The pore volume of MA-n sample was also enlarged from 0.22 (MA-1) to 0.27 (MA-4) then to 0.34 cm³ g⁻¹ (MA-6), close to that of form-like or mesoporous MgO (0.24–0.37 cm³ g⁻¹).^{11, 21} When the sample was carbonized below 773 K, they contained a lot of small pore with the size smaller

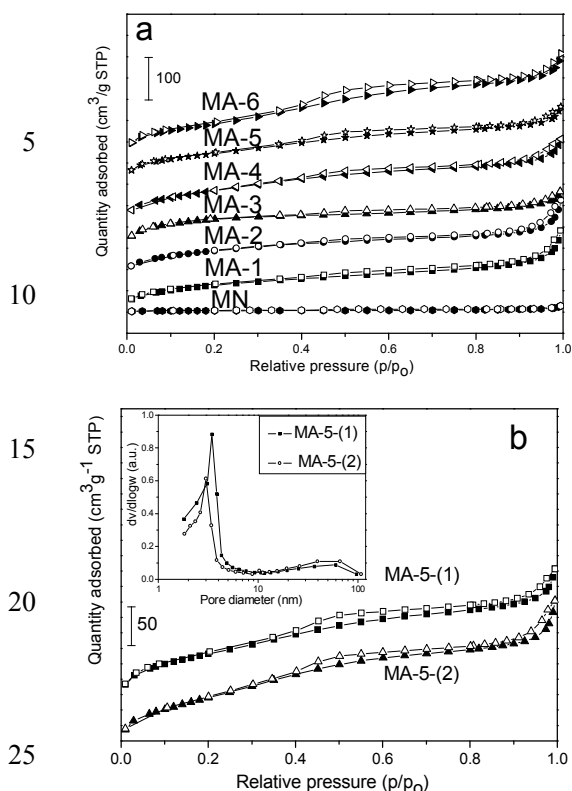


Fig. 3 The nitrogen adsorption-desorption isotherms of (a) MA-n and MN samples, (b) two MA-5 samples.

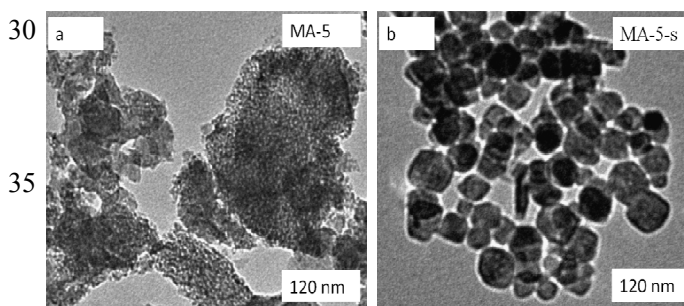
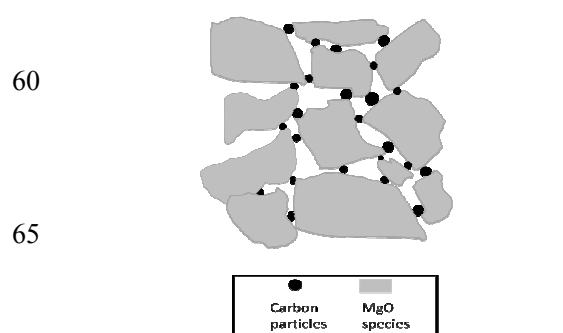


Fig. 4 TEM images of (a) MA-5 and (b) MA-5-s samples.

than 2 nm (Fig. 5a and 5b). For those carbonized above 773 K, the pores with the size of about 3 nm became the majority and the pore size distribution narrowed down as shown in Fig. 5a, which is similar to the report on mesoporous MgO,¹¹ but different from that of foam-like MgO where some macroporous pores were detected.¹⁸ Unlike nonporous MgO nanoparticulates losing its half surface area as the calcination temperature rose from 773 to 873 K,³⁰ MA-6 sample prepared at 873 K still had a large surface area (336 m² g⁻¹) similar to that of MA-4 (317 m² g⁻¹). This peculiar phenomenon is understandable since carbon adulterants are embedded in the composite to separate MgO nanoparticles and prevent their aggregation (Scheme 1).

Apart from carbonization temperature, we have explored other means of affecting the synthesis of porous MgO. In the survey experiments, magnesium acetate was thermally treated in various conditions. As the acetate was carbonized in tube furnace instead



Scheme 1. Separation of MgO particles by carbon-insertion.

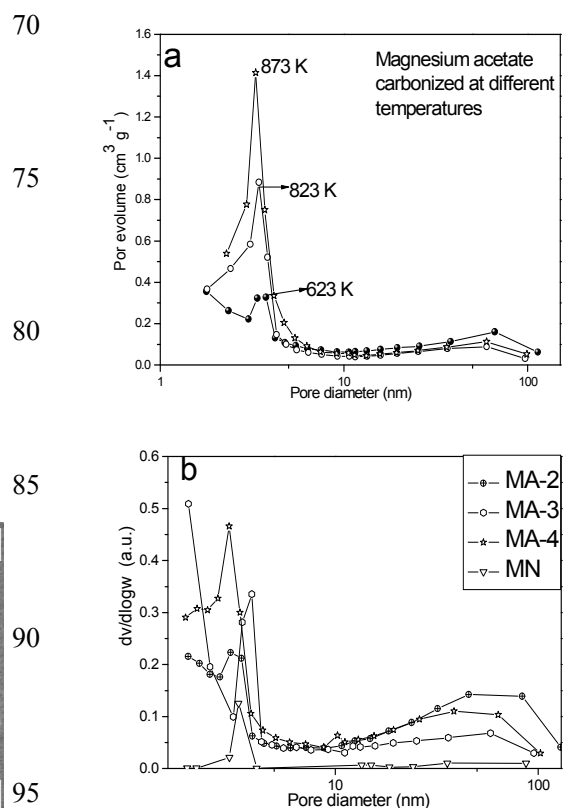


Fig. 5 The pore size distribution of magnesium acetate carbonized at different temperatures.

of u-type reactor, the resulting MA-5t sample exhibited a 25% reduced surface area and pore volume, and the application of Scherrer's formula to the wide-angle XRD diagrams suggested the domain sizes of 17±2 nm, which was larger than that of MA-5 (7±2 nm) though these values should be regarded as rough estimates only because of the limited accuracy of Scherrer's formula. Changing the carrier gas from N₂ to air in the tube furnace made the sample of MA-5t-a to have a further reduced pore volume accompanied with enlarged pore size and crystallites sizes, and its surface area was reduced about 80% (Table 1). In case the carbonization in u-type reactor was under N₂ atmosphere rather than N₂ flow, the resulting MA-5-s sample had a large pore size (23 nm) and a dramatically declined surface area (35 m² g⁻¹), while many large particles with the size of 35-55 nm appeared in its TEM image (Fig. 4b). If the acetate salt in u-type reactor was calcined in air flow instead of N₂, the obtained MA-5-a sample had a surface area reduced from 300 to 148 m² g⁻¹ (Table 1).

Similar difference was also found in the sample prepared at 623 K, MA-1-a owned a smaller surface area ($135 \text{ m}^2 \text{ g}^{-1}$) than MA-1 (235 $\text{m}^2 \text{ g}^{-1}$), further improving the superiority of carbonization to calcinations in preparing porous MgO sorbent from magnesium acetate.

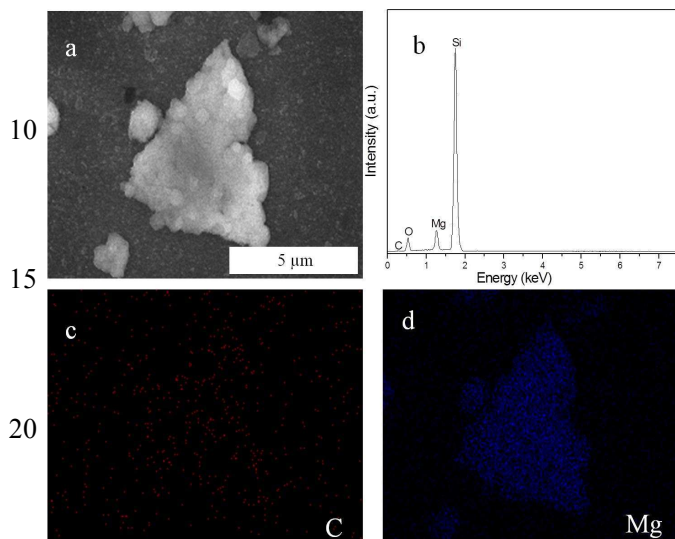


Fig. 6 (a) SEM images, (b) EDX spectrum, and (c, d) x-ray mapping of MA-5 sample in which the magnification is 10000.

All of MA-n samples are colored (Fig. S1), due to the existence of carbon particles formed in the carbonization of acetate,¹³ but the sample of MN prepared from $\text{Mg}(\text{NO}_3)_2 \cdot 6\text{H}_2\text{O}$ without carbon appeared a white color. In case MA-5 sample was dissolved in acid solution (Fig. S2), lots of carbon particles would suspend in solution while none was found in that of MN sample. According to the result of elementary analysis, the carbon content of MA-n was gently decreased from 8.2% to 1.8% as the carbonization temperature rose from 623 to 873 K (Table 1), while their surface C/Mg ratio increased from 1.4 to 4.1 then to 2.9 according to XPS analysis (Table S1), implying the possible migration of carbon components toward the external surface of sample. The carbon nanoparticles were embedded but sparsely distributed in MA-5 sample (Scheme 1) therefore an obvious contrast was observed in the magnesium and carbon element face mapping of MA-5 (Fig. 6), while a relatively compact and well-proportioned carbon mapping appeared on MA-1 sample because of its large carbon content (Fig. S3). Among the three samples carbonized at 823 K, MA-5-s had larger carbon content (4.3%) than that of MA-5 (2.5%) due to the absence of sweep gas flow, while the MA-5-t exhibited the smallest value (0.75%) since it was prepared flatwise in tube furnace. Such discrepancy in carbon content is a result due to the effects of purge gas flow as aftermentioned.

The calcined sample MA-5-a was carbon-free as expected, but its analogue MA-1-a owned a considerable carbon content (5.1%) and the yellow-brown color. Apparently, carbon precursors are also produced in the calcination of magnesium acetate in u-type reactor below 623 K though they are finally removed at high temperature. The average particle sizes were estimated from the Scherrer equation to be about 9.2 and 7.6 nm for MA-5-a and MA-1-a sample, larger than that of MA-5 (7.0 nm) and MA-1

(4.7 nm), respectively. These differences are understandable because MgO nanoparticles contact each other and easily aggregate at high temperature without carbon adulterants.³¹ It fails to create porous MgO in the thermal treatment of magnesium nitrate at 823 K, probably due to the special decomposition path in which the formed MgO particles are easily aggregated,³² and the resulting sample MN only showed a very small surface area ($11 \text{ m}^2 \text{ g}^{-1}$) and pore volume ($0.01 \text{ cm}^3 \text{ g}^{-1}$, Table 1). A Scherrer analysis of MN sample revealed the nanoparticles sizes of 54 nm.

Adsorption of CO_2 by porous MgO at 473 K

Both instantaneous and static CO_2 adsorption methods were used to assess the actual performance of MA-n composites. The CO_2 concentration in gas flow is about 5% in the instantaneous adsorption at 473 K, and the contact time between the whole sorbent bed and CO_2 is shorter than 2 s, which will inevitably suppress the capability of sorbent.^{13, 29} MA-n samples were efficient to capture CO_2 at 473 K except MA-1, and their capacity rose from 21 to 29 mg g^{-1} (Table 1), 4 times higher than that of common MgO (about 4 mg g^{-1}).²¹ In contrast, MN sample adsorbed the least of CO_2 (4.2 mg g^{-1}) at 473 K because of its small surface area and the large crystallite size (Table 1). When the adsorption was carried out at 423 K, more CO_2 (39.0 mg g^{-1}) could be captured by MA-5 sorbent but MN showed a similar capacity (4.8 mg g^{-1}) to that at 473 K (Fig. 7).

The result of instantaneous adsorption is confirmed by CO_2 adsorption isotherm, MA-5 sample trapped the CO_2 of 44.8 mg g^{-1} in the static adsorption at 473 K (Fig. 8a), exceeding that in instantaneous adsorption (27.7 mg g^{-1}). When the static adsorption was carried out at 423 K, the MA-5 sample adsorbed 51.3 mg g^{-1} of CO_2 , more than that of foam-like MgO prepared using surfactant templates (44.6 mg g^{-1} at 423 K)²¹ and the MgO-based sorbent promoted with K_2CO_3 (46 mg g^{-1} at 373 K).¹⁴ As demonstrated in Fig. 8a, the CO_2 uptakes increased with the increased pressure and the decreased temperature since CO_2 adsorption is an exothermic process. In addition, the isosteric heats of CO_2 adsorption on MA-5 sample is calculated from the CO_2 isotherms measured at 423 and 473 K. In case that 4 $\text{cm}^3 \text{ g}^{-1}$ (STP) of CO_2 was adsorbed on MA-5, an adsorption heat of 57.8 KJ mol^{-1} could be identified, while lower adsorption heat of 23.5 KJ mol^{-1} was found as the quantity adsorbed reached 15 $\text{cm}^3 \text{ g}^{-1}$ (STP), (Fig. 8b). These variations reflect the existence of different basic sites on sample.²¹

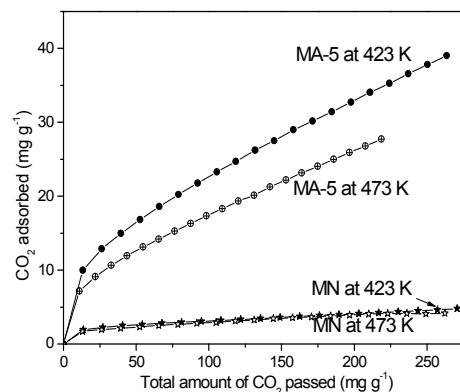


Fig. 7 The accumulative CO_2 adsorption curves at 423 and 473K on MA-5 and MN samples.

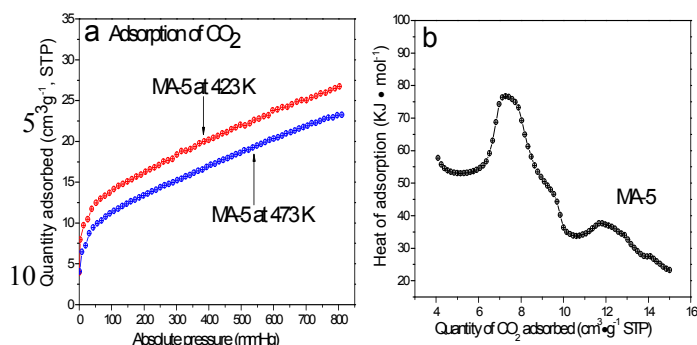


Fig. 8 The isotherms (a) and isosteric heat (b) of CO₂ adsorption on MA-5 sample.

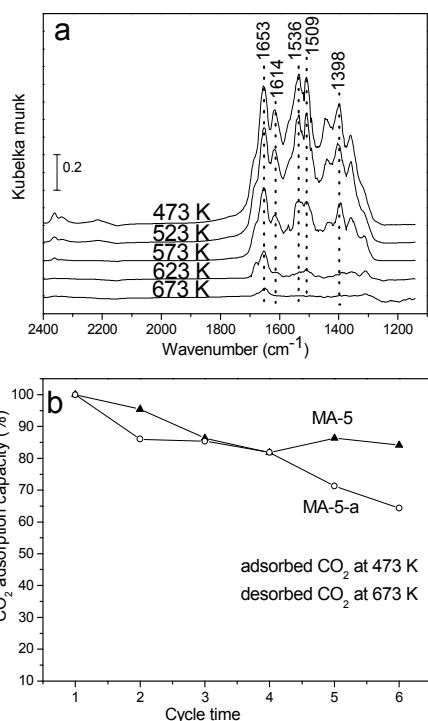


Fig. 9 The FTIR spectra (a) of CO₂ adsorbed on MA-5 and cyclic CO₂ adsorptions of MA-5 and MA-5-a (b).

On the FTIR spectrum of MA-5 sample adsorbed CO₂ at 473 K (Fig. 9a), bulk-like carbonate species appeared between 1250 and 1650 cm⁻¹,³³ among them the 1653 cm⁻¹ band of asymmetric stretching vibrations of O-C-O indicates bidentate carbonate or bicarbonate species.³⁴ The sharp band at 1536 cm⁻¹ associated with a band at 1509 cm⁻¹ represents the asymmetric vibration of monodentate carbonate species,²³ the band at 1398 cm⁻¹ denotes the O-C-O symmetric stretching vibration of the species.²³ As the temperature increased to 673 K, the bands of monodentate carbonate species disappeared while the bands of bidentate species dramatically declined on the spectrum. It is clear that almost of the CO₂ adsorbed in the composite desorbs at 673 K, which results from the proper basic strength of MA-5 sorbent but differs from foam-like MgO where monodentate bands survived at 773 K.¹⁵ As the result, MA-5 composite showed a high ability in the six cycles of adsorption (473 K)-desorption (673 K). Its relative adsorption capacity declined from 100% to 84% (Fig. 9b),

slightly better than that of foam magnesia on which about 80% of initial capacity remained,¹⁵ but superior to MA-5-a whose residual activity was about 65%.

Carbon adulterants in porous MgO sorbent impact the instantaneous CO₂ adsorption at 473 K. Due to absence of carbon, MA-5t-a sample only trapped less CO₂ at 473 K (7.5 mg g⁻¹) than MA-5t (15 mg g⁻¹) and MA-5 (27 mg g⁻¹) because its surface area (42 m² g⁻¹) was smaller than that of MA-5t (225 m² g⁻¹) and MA-5 (300 m² g⁻¹). Similarly, MA-5-a showed a CO₂ adsorption capacity (19.8 mg g⁻¹, Table 1) 28% smaller than MA-5. Carbonization in tube furnace made MA-5t sample to have a capacity 55% lower than that of MA-5, due to its less carbon content and larger MgO particles size. In contrast, MA-5-s sample only exhibited a weak capability (8.1 mg g⁻¹) to adsorb CO₂ at 473 K since the carbon wrapped the MgO particles as aforementioned and the formation of large particles (23.5 nm, Table 1), which prejudices CO₂ adsorption.^{11, 19}

Carbonization temperature affects the distribution of carbon in MA-n samples and their CO₂ adsorption performances. The MgO particles of MA-1 were covered by carbon precursors formed at 623 K so this yellow sample (Fig. S1) hardly adsorbed CO₂ at 473 K (less than 1 mg g⁻¹). These carbon precursors in MA-2 sorbent gently formed carbon at 673 K hence lots of black spots appeared on the yellow sample. Also, its surface area was enhanced 15% and the CO₂ adsorption capacity dramatically rose to 20.8 mg g⁻¹ at 473 K, resulting from the exposure of major MgO particles for CO₂. For MA-3 sorbent carbonized at 723 K, its color became black accompanied with a 16% larger surface area and a 27% higher CO₂ adsorption capability. In general MgO nanoparticles tend to aggregate at high temperature driven by the minimization of surface energy³⁵, which seems inconspicuous here since the crystallite sizes and CO₂ adsorption capacity of MA-3, MA-4 and MA-5 samples were similar (Table 1). Carbonization at 873 K slightly further increased the surface area of MA-6 meanwhile reduced its carbon content, ulteriorly expanding the exposure of MgO hence it captured 28.9 mg g⁻¹ of CO₂ at 473 K (Table 1). To understand this achievement, it is necessary to calculate the CO₂ adsorption by MgO at 473 K. If (as is probable on energetic grounds) the surface of MgO was a 100 plane, then it would contain 11.3 ions of magnesium and 11.3 ions of oxygen per nm².²⁴ Considering the cross-sectional area of CO₂ (18-20 Å² molecule⁻¹), the monolayer capacity of the surface should not exceed ca. 5 molecules nm⁻² (8.3 μmol m⁻²) if these CO₂ were chemisorbed in bidentate mode.^{24, 34} On the other hand, there are three types of basic sites on the surface of MgO, hydroxyl groups, the oxygen in Mg²⁺ and O²⁻ pairs, and the low coordination oxygen anions.²³ Among them only those located in some particularly energetic and reactive minority sites of MgO plane (e.g., edge, corner, and defect sites)³⁴ can adsorb CO₂ at 473 K, and this ratio is no more than 37% on the MgO sample prepared from magnesium methylate with a surface area of 112 m² g⁻¹.²⁴ Based on this assumption the theoretical CO₂ adsorption capacity of MgO at 473 K is estimated to be about 0.14 mg m⁻². MA-4, MA-5 and MA-6 samples had a capacity of about 0.09 mg m⁻² in the CO₂ adsorption at 473 K (Table 1), same as the report on the MgO prepared from magnesium methoxide,²⁴ equaling to 64% of the theoretical value. The capability of MA-5-a sample was 0.13 mg m⁻² under the same condition, and the difference

between MA-5 and MA-5-a may result from the blockage of small pores by the inserted carbon, as that observed in the interpenetrated MOFs,³⁶ but further investigation is required.

Discussion

5 Three factors ensure the fabrication of novel porous MgO, named as “carbon insertion”, derived from carbonization of magnesium acetate. The first one is the carrier gas flow purging the gaseous products of acetate decomposition. Formation and release of gaseous products such as CO₂, moisture and acetone will leave
10 behind some pores in the primary MgO particles.^{26, 35} Although the variation of gas flow speed in the range of 10-50 ml min⁻¹ had an unobvious influence on the actual CO₂ adsorption of resulting sample (Fig. S4), the MA-5-s sample prepared in N₂ atmosphere rather than N₂ flow lacked pore in its TEM image (Fig. 4b) so
15 that it only trapped 8 mg g⁻¹ of CO₂ at 473 K, much less than MA-5 does (27 mg g⁻¹). Also, its surface area (35.3 m² g⁻¹) was 88% smaller than that of MA-5 since it consisted of the relatively large particles with the sizes of 36~60 nm (Fig. S5). Presumably, this is because the co-existed carbon components wrap the MgO.
20 The second factor affecting the carbonization of magnesium acetate is the contact manner of gas flow with the salt. When the salt was placed in a quartz tube that is placed flatwise in tube furnace, the resulting composite MA-5t had a 25% smaller surface area and 48% reduced CO₂ adsorption capability at 473 K
25 in comparison with MA-5 (Table 1). These differences originate from altered contacting manner of gas flow with the salt: the gas adequately mixed with the solid in the u-type reactor, sweeping the particles and fragmenting the aggregate into individual MgO particles that are free from strong interparticle contacts.³² The
30 speed of gas flow exceeded 4 m s⁻¹ hence hot steam was removed quickly so that crystallization took place, but crystallite sintering did not take place.²⁵ As the result, the crystallites sizes of MA-n samples were smaller than 8 nm (Table 1). In contrast, the gas stream purged above the salt in the tube furnace, sweeping the
35 external surface of solid hence the inner part of the salt was carbonized somewhat statically to form large MgO particles. This inference is supported by the difference between two calcined samples MA-5-a and MA-5t-a, the former has an obvious smaller particle size and larger surface area than that of the latter (Table
40 1), demonstrating the nonnegligible influence of contact manner of carrier gas. The third important factor for carbonization of magnesium acetate is the suitable temperature, at which the carbon adulterants can be formed, and embedment of carbon in MgO particles will fabricate lots pores or gaps (Scheme 1).
45 Otherwise, the carbon precursors will wrap MgO particles and the sorbent is inactivated like MA-1 in adsorbing CO₂ at 473 K.
Carbon insertion enables MgO particles to be well accessible. For instance, to fabricate a 10 nm cylinder MgO like that prepared through replica with pore size of 7 nm and wall
50 thickness of 3.1 nm,²² it theoretically requires MgO of 416 nm³ and the exposed surface area is about 261 nm² so that its S/V ratio will be 0.63. If this amount of MgO was dispersed as that on mesoporous carbon with the particles size of 13.1 nm,¹⁶ it would have the exposed surface area of 165 nm² assumed they were
55 equally mixture of hemisphere and cube hence its S/V ratio is 0.40. In case they were existed in the state of MA-5 with the particles size of 7 nm, they would have the exposed surface area

of 307 nm² with the S/V ratio of 0.74. In fact, the surface area of 250~280 m² g⁻¹ was reported on the mesoporous MgO
60 synthesized by exotemplating using CMK-3 carbon,^{20, 22} smaller than that the value of MA-5 (300 m² g⁻¹, Table 1).

The capability of MgO to capture CO₂ at 473 K depends on the number of accessible strong basic sites, which is related with but not limited to the surface area of MgO because the exposed MgO
65 should keep its original crystal structure where the defects provide the required basic active sites.²⁰ The surface state of MgO, involving the number and the distribution of structural defects and vacant sites as well as coordinative unsaturated surface sites
70 ³⁷, has a significant influence on its actual basicity so that the final reactivity of MgO strongly depends on the preparation method and the precursor used³⁸. Some MgO-supported sorbents had a large surface area where MgO was well dispersed, but the capability of MgO was declined more or less since the well-dispersed guest might lose its original crystal meanwhile the
75 surface interaction between the support and MgO would consume part of the guest.³⁹ For the porous MgO with non-ordered pore structure,²¹ only the MgO exposed could contact with CO₂ while those located in the inner layers could not, which also reduced the capability of the sorbent. Actually, there is no CO₂ adsorption at
80 473 K reported on those ordered mesoporous MgO,^{22, 29, 31} probably due to the lack of strong basic sites as that observed previously on many MgO sorbents.^{17, 18, 39} Here the co-existed carbon particles are utilized as the special adulterant to separate the MgO nanoparticles through the *in situ* insertion, enhancing
85 the surface area and exposure of MgO, Carbon has a molecular weight less than magnesium, and these adulterants are survived from the sweep of carrier gas with high speed so that their amount and position can be optimized⁴⁰ (only about 2% of carbon was detected in MA-5 sample). Since the carbon particles are *in situ* formed with and inserted into those MgO particles, the adulterants will mix with MgO hand in glove to prevent the contact and aggregation of MgO particles. Moreover, carbon adulterant is inert for MgO avoiding unnecessary interaction so that MgO particles are separated keeping their original irregular
95 and defective surfaces, which is beneficial for the exposure of strong adsorptive sites on MgO.^{13, 20} Thanks to the new concept of “carbon insertion”, new porous MgO samples with a surface area of 200~300 m² g⁻¹ is simply obtained through a solvent-free thermal process, and they exhibit an excellent performance in the
100 CO₂ adsorption at 473 K. Especially, the existence of carbon in MA-n composites not only promoted the pore-creating, but also affected the CO₂ adsorption more or less therefore MA-5 sample displayed a good performance in cycle adsorption of CO₂ at 473 K and desorption at 673 K. Concerning the possible deactivation
105 of MA-n composite, the main reason will be the loss of carbon adulterators caused in two situations. One is the continuously purge of MgO-C composite by inert carrier gas such as N₂ for a long time, in which the carbon nanometer particles will be gently moved, migrated and finally removed out, remaining the MgO
110 particles to be aggregated. Another situation is to use this MgO-C composite in the oxygen-containing gas flow at high temperature, in which the carbon particles will be oxidized and the MgO particles aggregate together. Studying the prevention of MgO-C composites from deactivation is the next frontier.

115 Fabrication of porous MgO sorbent through carbon insertion

manner is also cost-effective and environment benign since it avoids the use of template and toxic solvent, and the inherent carbon source of acetate is used to be the adulterants of MgO particles while the emission of CO₂ and volatile organic compound like acetone is reduced. Moreover, the ratio of MgO to carbon in this porous sorbent can reach 49:1, much larger than that of common MgO-supported or mixed sorbent.^{8, 18}

Conclusion

In conclusion, a very simple and scalable “carbon insertion” pathway has been explored for preparation of porous MgO sorbent using carbonization of magnesium acetate.

(1) The porous MgO sorbent with a high surface area above 200 m² g⁻¹ could be conveniently fabricated from carbonization of magnesium acetate in the range of 673–873 K. Especially, the composite prepared at 823 K had a high BET surface area of 300 m² g⁻¹ and mesoporous structure with no long-range order. And it contained about 2% of carbon.

(2) These porous MgO sorbents were able to capture CO₂ in the instantaneous adsorption at 473 K, up to 28 mg g⁻¹. And the sample prepared at 823 K kept the 84% of initial adsorption capacity in 6th cycle adsorption at 473 K.

(3) Carbonization temperature, gas flow and its contact manner with the salt are three crucial factors to determine the property and performance of porous MgO sorbent derived from thermal decomposition of magnesium salt.

(4) Apart from the advantage of solvent-free, simple and cost-effective, this “carbon insertion” new method utilizes the newly-formed carbon in carbonization of acetate to separate the co-existed MgO nanoparticles, avoiding their aggregation. Same strategy is expected to be applied for synthesis of other functional materials.

Acknowledgements

Financial support from NSF of China (21173117 and 21273106), Grant 2008AA06Z327 from the 863 Program of the Ministry of Science and Technology of China, scientific research foundation of graduate school and Analysis Center of Nanjing University is gratefully acknowledged.

Notes and references

^a Key Laboratory of Mesoscopic Chemistry of MOE, College of Chemistry and Chemical Engineering, Nanjing University, Nanjing 210093, China.

Fax: 0086-25-83317761; Tel: 0086-25-83595848; E-mail:

jhzhu@nju.edu.cn

^b College of Chemistry & Chemical Engineering, Nanjing University, Nanjing 210093, China.

^c Ecomaterials and Renewable Energy Research Center (ERERC), Nanjing University, Nanjing 210093, China

† Electronic Supplementary Information (ESI) available: See DOI: 10.1039/b000000x/

- 1 R. G. Watts, *Global Warming and the Future of the Earth*, Morgan & Claypool Publishers, Denver, 2007.
- 2 J. Liu, P. K. Thallapally, B. P. McGrail, D. R. Brown, J. Liu, *Chem. Soc. Rev.*, 2012, **41**, 2308.
- 3 C. S. Song, *Catal. Today*, 2006, **115**, 2.
- 4 S. Bachu, *Prog. Energy Combust. Sci.*, 2008, **34**, 254.
- 5 X. S. Yin, S. P. Li, Q. H. Zhang, J. G. Yu, *J. Am. Ceram. Soc.*, 2010, **93**, 2837.
- 6 A. Veawab, P. Tontiwachwuthikul, A. Chakma, *Ind. Eng. Chem. Res.*,

1999, **38**, 3917.

- 7 H. Gupta, L. S. Fan, *Ind. Eng. Chem. Res.*, 2002, **41**, 4035.
- 8 H. Jeon, Y. J. Min, S. H. Ahn, S.-M. Hong, J.-S. Shin, J. H. Kim, K. B. Lee, *Colloid Surf. A: Physicochem. Eng. Aspects*, 2012, **414**, 75.
- 9 C. L. Yan, D. F. Xue, *J. Phys. Chem. B*, 2005, **109**, 12358.
- 10 M. J. Climent, A. Corma, S. Iborra, M. Mifsud, *J. Catal.*, 2007, **247**, 223.
- 11 S.-W. Bian, J. Baltrusaitis, P. Galhotra, V. H. Grassian, *J. Mater. Chem.*, 2010, **20**, 8705.
- 12 M. Bhagiyalakshmi, P. Hemalatha, M. Ganesh, P. M. Mei, H. T. Jang, *Fuel*, 2011, **90**, 1662.
- 13 Y. Y. Li, K. K. Han, W. G. Lin, M. M. Wan, Y. Wang, J. H. Zhu, *J. Mater. Chem. A*, 2013, **1**, 12919.
- 14 L. Li, X. Wen, X. Fu, F. Wang, N. Zhao, F. K. Xiao, W. Wei, Y. H. Sun, *Energ. Fuel.*, 2010, **24**, 5773.
- 15 K. K. Han, Y. Zhou, Y. Chun, J. H. Zhu, *J. Hazard. Mater.*, 2012, **203–204**, 341.
- 16 L. She, J. Li, Y. Wan, X. Yao, B. Tu, D. Zhao, *J. Mater. Chem.*, 2011, **21**, 795.
- 17 Y. Wang, J. H. Zhu, J. M. Cao, Y. Chun, Q. H. Xu, *Micropor. Mesopor. Mater.*, 1998, **26**, 175.
- 18 Z. Y. Wu, Q. Jiang, Y. M. Wang, H. J. Wang, L. B. Sun, L. Y. Shi, J. H. Xu, Y. Wang, Y. Chun, J. H. Zhu, *Chem. Mater.*, 2006, **18**, 4600.
- 19 A. Zukal, J. Pastva, J. Cejka, *Micropor. Mesopor. Mater.*, 2013, **167**, 44.
- 20 S. Coluccia, A. Barton, A. J. Tench, *J. Chem. Soc., Faraday Trans. 1*, 1981, **77**, 2203.
- 21 K. K. Han, Y. Zhou, W. G. Lin, J. H. Zhu, *Micropor. Mesopor. Mater.*, 2013, **169**, 112.
- 22 J. Roggenbuck, M. Tiemann, *J. Am. Chem. Soc.*, 2005, **127**, 1096.
- 23 J. Hu, K. Zhu, L. Chen, C. Kubel, R. Richards, *J. Phys. Chem. C*, 2007, **111**, 12038.
- 24 S. J. Gregg, J. D. Ramsay, *J. Chem. Soc. A*, 1970, 2784.
- 25 S. Utamapanya, K. J. Klabunde, J. R. Schlup, *Chem. Mater.*, 1991, **3**, 175.
- 26 A. Hassanzadeh, J. Abbasian, *Fuel*, 2010, **89**, 1287.
- 27 E. G. Derouane, Z. Gabelica, R. Hubin, M. J. Hubin-Franskin, *Thermochimica Acta*, 1975, **11**, 287.
- 28 A. M. M. Gadalla, *Thermochimica Acta*, 1984, **74**, 255.
- 29 M. Bhagiyalakshmi, J. Y. Lee, H. T. Jang, *Int. J. Greenhouse Gas Control.*, 2010, **4**, 51.
- 30 J. M. Montero, D. R. Brown, P. L. Gai, A. F. Lee, K. Wilson, *Chem. Eng. J.*, 2010, **161**, 332.
- 31 J. Roggenbuck, C. Koch, M. Tiemann, *Chem. Mater.*, 2006, **18**, 4151.
- 32 T. J. Gardner, G. L. Messing, *Thermochimica Acta*, 1984, **78**, 17.
- 33 A. M. Ruminski, K.-J. Jeon, J. J. Urban, *J. Mater. Chem.*, 2011, **21**, 11486.
- 34 G. A. H. Mekhemer, S. A. Halawy, M. A. Mohamed, M. I. Zaki, *J. Phys. Chem. B*, 2004, **108**, 13379.
- 35 H. Niu, Q. Yang, K. Tang, Y. Xie, *Micropor. Mesopor. Mater.*, 2006, **96**, 428.
- 36 R. Babarao, C. J. Coghlan, D. Rankine, W. M. Bloch, G. K. Gransbury, H. Sato, S. Kitagawa, C. J. Sumby, M. R. Hill, C. J. Doonan, *Chem. Commun.*, 2014, **50**, 3238.
- 37 M. Anpo, S. C. Moon, K. Chiba, *Res. Chem. Intermedi.*, 1993, **19**, 495.
- 38 J. Take, N. Kikuchi, Y. Yoneda, *J. Catal.*, 1971, **21**, 164.
- 39 Y. M. Wang, Z. Y. Wu, Y. L. Wei, J. H. Zhu, *Micropor. Mesopor. Mater.*, 2005, **84**, 127.
- 40 F. N. Gu, F. Wei, J. Y. Yang, Y. Wang, J. H. Zhu, *J. Phys. Chem. C*, 2010, **114**, 8431.
- 41 F. Wei, J. Y. Yang, L. Gao, F. N. Gu, J. H. Zhu, *J. Hazard. Mater.*, 2009, **172**, 1482.